JOC The Journal of Organic Chemistry

Article

pubs.acs.org/joc

Theoretical Insight into the Mechanism of Gold(I)-Catalyzed Rearrangement of 2-Propargyl 2*H*-Azirines to Pyridines

Lu Jin, Yong Wu,* and Xiang Zhao*

Institute for Chemical Physics and Department of Chemistry, School of Science, Xi'an Jiaotong University, Xi'an 710049, China

Supporting Information

ABSTRACT: The title reaction is investigated in detail theoretically using density functional theory. After 5-*endo*-dig cyclization by nucleophilic attack, five possible pathways are taken into account in this work: direct ring expansion followed or accompanied by proton-transfer (paths A and B, respectively), 1,3-cationic migration (path C), proton-transfer before ring expansion (path D), and processing via a gold-nitrene (path E). Results indicate that the reaction would undergo the favored sequential pathway (path A) rather than other pathways. Moreover, the concerted mechanism (path B), which is designed to account for the selectivity of product in the experiment, would be unlikely in the reaction. The selectivity of product could be explained by the hindrance of ligand (*t*-BuXPhos) and the stability of the carbocation. Moreover, the binding energy of product complexes could account for the observed reaction rate.

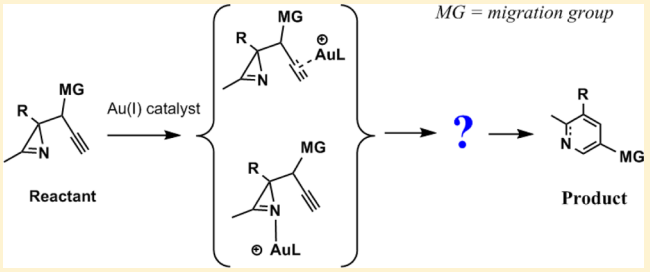

1. INTRODUCTION

The smallest nitrogen-containing unsaturated heterocycles with a C═N double bond in a three-membered ring, 2*H*-azirines, have been extensively studied in natural products and synthetic applications.[1,2] It is easy to form 2*H*-azirines using the Neber reaction or other strategies.[3] Because of the intrinsic strain of the three-membered ring, these compounds can undergo facile ring-opening. As a source of nitrenes, electrophiles, dienophiles, and dipolarophiles, 2*H*-azirines can be used for N-heterocycle syntheses, such as for indoles, pyrroles, isoxazoles, and pyridines. In the past decade, transformation of 2*H*-azirines to other chemicals has attracted much attention, and many elegant methods have been developed.[4]

For the transformation of 2*H*-azirines, there are still limited methods to break the C−N single bond.[1,4,5] For example, 2*H*-azirines can be considered as synthetic equivalents of alkenyl nitrenes under organometallic catalysis. This type of transformation is available by using Rh(I), Fe(II), and Cu(II) catalysts.[5] Both experimental predictions and computational results indicate that a metal-nitrene reactive intermediate can occur in these reactions.[5] On the basis of experimental results reported by Narasaka and Zheng, Yan and co-workers systematically studied the ring-expansion mechanism of 2-aryl-2*H*-azirines to 2,3-disubstitued indoles using the density functional method (DFT).[5b] They found that, in $FeCl_2$-catalyzed reactions, it is easy to undergo ring-opening to form an iron-nitrene intermediate on the quintet potential energy surface, and the rate-determining step is associated with ring-closure (C−N bond formation), whereas the rate-determining step changes to the ring-opening of azirine to afford a ruthenium-nitrene intermediate in the $Ru_2(O_2CCF_3)_4$-catalyzed reaction on the singlet potential energy surface (Scheme 1).

Scheme 1. Rearrangement Mechanism of 2-Aryl-2*H*-azirines to 2,3-Disubstitued Indoles via a Metal-Nitrene Intermediate

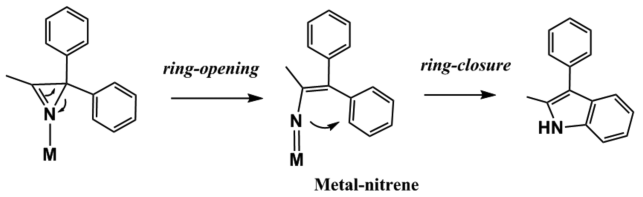

Over the past decade, homogeneous gold(I)-catalyzed organic transformation has attracted much attention in experimental[6] and theoretical[7] studies due to the unique ability of gold to coordinate with unsaturated bonds. Recently, Gagosz and co-workers reported a novel gold(I)-catalyzed synthesis of functionalized pyridines from alkynyl-containing 2*H*-azirines (Scheme 2).[8] According to their experimental observations, sequential (path A) and concerted (path B) mechanistic pathways were attempted for the reaction. First, the nucleophilic addition of nitrogen to gold(I)-activated alkyne leads to five-membered ring intermediate **2**. Then, followed or accompanied by 1,2-migration of neighboring group, three-membered ring expansion can finish the reaction. Although they proposed the concerted mechanism to account for the selectivity of product when a substitution is placed at the propargylic position (C3), they suggested that both mechanisms could operate because it is difficult to rule out either individual mechanism from the experimental results.

It is crucial to understand the details of the reaction mechanisms, which can explain the experimental results and

Received: January 26, 2015
Published: March 11, 2015

DOI: 10.1021/acs.joc.5b00180
J. Org. Chem. 2015, 80, 3547−3555

Scheme 2. Possible Reaction Pathways for the rRearrangement of 2-Propargyl 2*H*-Azirine

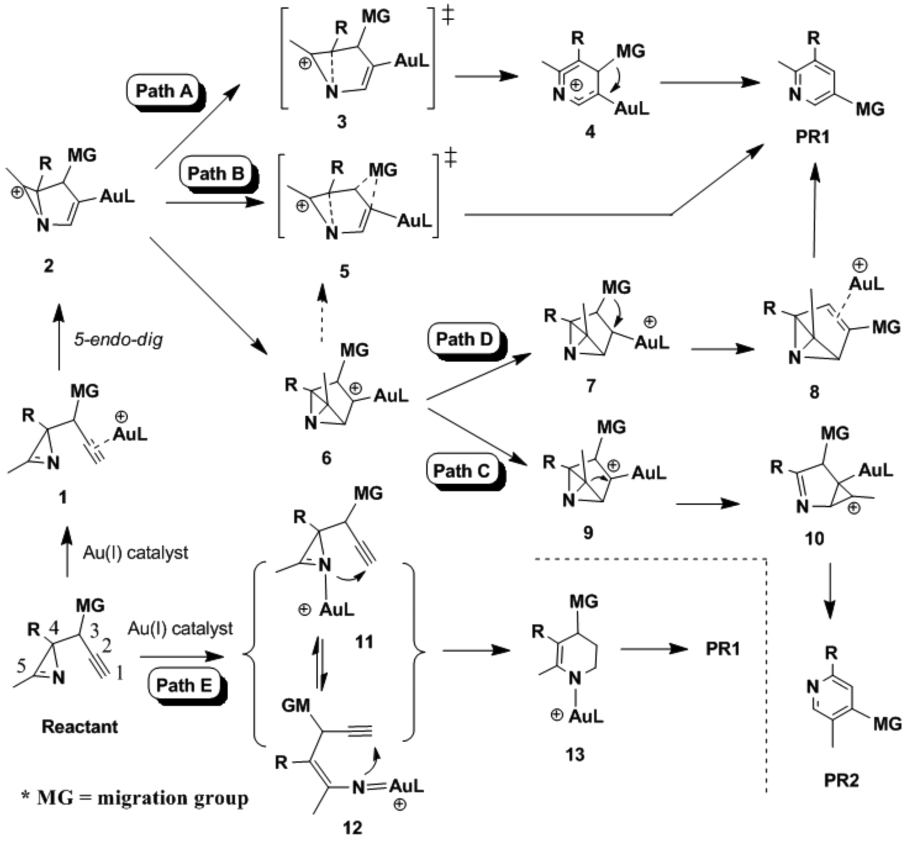

facilitate the development of practical methodologies for synthetic chemistry. Similar to the title reaction, gold(I)-catalyzed cycloisomerization of 1,5-enynes containing a cyclopropene moiety was experimentally studied by Wang et al. and computationally verified by Li et al.[9] Both results support the occurrence of competitive 1,3-cationic alkylidene migration in the rearrangement after 1,5-*endo*-dig cyclization, rendering two possible products depending on the substituent groups. In this sense, except for the proposed "sequential" and "concerted" mechanisms noted above, the process (path C in Scheme 2) via 1,3-cationic alkylidene migration should be checked in the title reaction. In this pathway, we found that intermediate **6**, in which two three-membered rings share one edge, could occur in the reaction (see the Results for details). We considered one more possible pathway in which 1,2-migration occurs prior to ring expansion (path D). Additionally, we also checked a possible pathway through a gold(I)-nitrene intermediate (**12**, path E). Accordingly, Scheme 2 depicts the five possible pathways promoted by one gold(I) catalyst.

Our motivation in this work is to clarify the detailed reaction process using pure computations and to examine which pathway would be more favorable to occur in the reaction. The spatial effect of a real ligand in the catalyst is also evaluated for the reaction. Additionally, it is interesting to understand the reactive intermediates, including the competition between the 2*H*-azirine moiety and alkyne for binding to the gold(I) catalyst and whether it is possible to form a gold-nitrene intermediate via opening of the three-membered ring.

2. COMPUTATIONAL DETAILS

All of the relevant geometries were fully optimized in the solvent (CH_2Cl_2) using the combination of PBE0 density functional theory[10] and the self-consistent reaction field (SCRF) theory. Recent assessment shows that PBE0 can suitably describe gold complexes.[11] The standard 6-311+G(d,p) basis set on nonmetal atoms and the Def2-TZVP basis set, including effective core potential (ECP) on Au atoms, were used for the model system (denoted as BS-I), whereas 6-31G(d,p) and Def2-SVP basis sets (denoted as BS-II) were used for the real system to reduce computational cost.[12] After geometry optimization, harmonic vibrational analyses were performed at the same level to confirm that each minimum has no imaginary frequency and that each transition state (TS) has only one imaginary frequency. The minimum energy path (MEP) was also traced using the intrinsic reaction coordinate (IRC)[13] method to ensure that each TS structure correctly links with two minima. The implicit IEF-PCM solvent model was adopted to evaluate solvent effect on the reaction in CH_2Cl_2 (ε = 10.125).[14] To match with the experimental conditions, all energies were corrected at 85 °C and 1 atm. Generally, compared to geometry, energy is sensitive to the computational method. Recently, a double-hybrid functional method (such as B2PLYP) including second-order perturbation energy was recommended for the energy computations.[15] In this sense, single-point energy calculations were carried out at the B2PLYP/BS-I level for the model system and the ONIOM(B2PLYP/BSI:PBE0/BS-I)//PBE0/BS-II level for the real system. Then, thermodynamic quantities were obtained by adding zero-point vibrational energies, thermal corrections, and entropy contributions to the single-point energies. Unless otherwise noted, relative Gibbs free energies (ΔG) at 85 °C are shown in this article. Furthermore, some electronic structures were analyzed by the natural bond order (NBO) method.[16] All computations were fulfilled with the Gaussian 09 program.[17] All three-dimensional structures were produced by the CYLview program.[18]

3. RESULTS AND DISCUSSION

3.1. Reaction Pathways for the Model System.

According to published experimental results,[8] the following reaction (Scheme 3) was selected in our work.

DOI: 10.1021/acs.joc.5b00180
J. Org. Chem. 2015, 80, 3547−3555

Scheme 3. Experimentally Reported Reaction (from Ref 8)

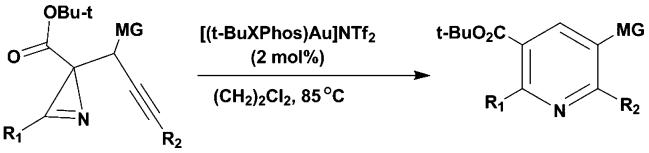

Herein, to reduce computational cost and provide a general mechanism, a model system in which the catalyst [(*t*-BuXPhos)-Au]$^+$ and CO_2Bu-t group were simplified to $[AuP(Me)_3]^+$ and CO_2Me was used for computations. Moreover, we only considered the model reaction where R_1 = CH_3, R_2 = H, and MG = H.

3.1.1. Formation of Reaction Complexes. Figure 1 shows that three possible reaction complexes could be formed in the initial stage of the reaction. Because of low catalyst loading and a large real ligand (*t*-BuXPhos), we ruled out the possibility of two gold(I) catalysts binding to one substrate. The nitrogen of the 2*H*-azirine moiety is more favorable than alkyne to interact with the gold(I) catalyst. As shown in the Supporting Information, the second-order stabilization energy (E^2) for the interaction of the lone-pair (LP) of nitrogen with antibonding of Au−P (σ^*_{Au-P}) is 87.99 kcal/mol in **CM3**, and second-order stabilization energies are 84.59 and 23.15 kcal/mol for $\pi_{C1=C2} \rightarrow \sigma^*_{Au-P}$ and back-donation of $d_{Au} \rightarrow \pi^*_{C1=C2}$ in **CM1**. Note that the starting reactant complex **CM1** is directly associated with the following cyclization, and its energy is therefore set to zero in this article.

As stated in the Introduction, detailed processes for three possible pathways (paths A, C, and D) of the title reaction are shown in Figure 2. Two other possible pathways (Scheme 2, structure 5 in path B and structure 12 in path E) could not be optimized on the potential energy surface with this computational method. As a π-acid catalyst, the gold(I) catalyst first activates alkyne in the reaction. After 5-*endo*-dig cyclization, path A is associated with direct ring expansion followed by 1,2-proton-transfer, whereas an alternative pathway is to form a tight intermediate (**a-IM-3**) in which two three-membered rings share one edge. Then, path C corresponds to the carbocationic shift, which could be detected in the rearrangement reaction of cyclopropene-containing 1,5-enyne, whereas path D is the process of 1,2-proton-transfer followed by ring-expansion.

3.1.2. Cyclization Pathways. As shown in Figure 3, two possible reaction types, 4-*exo*-dig and 5-*endo*-dig, could exist in the cyclization induced by the nucleophilic attack of the N atom on the C≡C triple bond. The $\Delta G^{\ddagger}$ (16.08 vs 35.06 kcal/mol) calculated indicates that the 5-*endo*-dig cyclization transition state **a-TS-1** should be more favorable than the 4-*exo*-dig cyclization transition state **b-TS**. Both imaginary frequencies mainly correspond to the C−N bond stretch modes. Note that it is strongly reversible for the 5-*endo*-dig cyclization from **CM1** to **a-IM-1** via **a-TS-1**. Similar to the case of cyclopropene-containing 1,5-enyne, the difference in ring strain between **a-TS-1** and **b-TS** could be responsible for the selectivity in the cyclization step. Therefore, it is less likely to undergo the 4-*exo*-dig cyclization.

For C−N bond formation in **a-TS-1**, the second-order stabilization energies (E^2) are 18.61 and 27.06 kcal/mol for $\pi_{C5=N} \rightarrow \pi^*_{C=C2}$ and LP(N) $\rightarrow \pi^*_{C1=C2}$, indicating that except for the lone-pair of nitrogen the C=N π bond of azirine also partially contributed to the nucleophilic addition. Therefore, from **CM1** to **a-TS-1**, the C1−C2 and C5−N bonds slightly elongate by 0.038 and 0.014 Å, respectively. The C1−N bond length is 2.028 Å, and its Wiberg bond index is 0.304, indicating that **a-TS-1** is a reactant-like (early) transition state.

After the reaction overcomes transition state **a-TS-1**, it offers the intermediate **a-IM1**. In **a-IM-1**, distances of C1−C5 and N−C1 are 2.550 and 1.474 Å, respectively. The bond angle of C1−C2−Au is 124.04°, revealing that the gold(I) catalyst completely binds to the C2 atom. IRC results show that the reaction simultaneously undergoes C1−N bond formation and a shift of the gold(I) catalyst toward the C2 atom in the 5-*endo*-dig process. We found that from **CM1** to **a-IM-1** the natural charge of the gold(I) catalyst decreases by ~0.23 e, whereas the C5 atom increases by ~0.18 e. It turns out that the formal positive charge should partially transfer from the gold(I) catalyst to the C5 atom, making the C5 atom the carbocation. Next, two possibilities are considered in our study, namely, direct ring expansion through sequential (path A) or concerted (path B) processes and ring-contraction through C1−C5 bond formation leading to gold carbenoid intermediate **a-IM-3**.

3.1.3. Direct Ring Expansion via Paths A or B. Obviously, the reaction can undergo C4−N ring cleavage due to the three-membered ring strain in **a-IM-1**. Figure 4 shows the sequential process (path A) and the corresponding relative free energies. In transition state **a-TS-2**, the C4−N bond is elongated to 1.812 Å, and its Wiberg bond index is reduced to 0.6114. $\Delta G^{\ddagger}$ is only 1.96 kcal/mol in this elementary step. Then, the plane intermediate **a-IM-2**, including a six-membered ring, is generated. The following

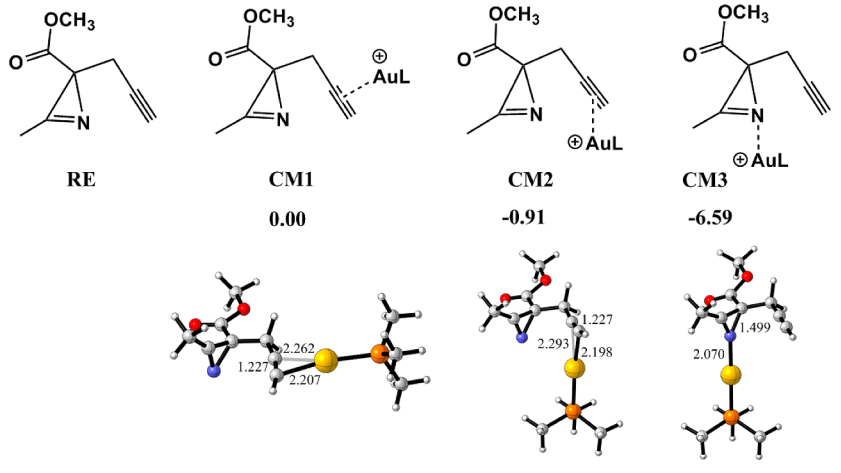

Figure 1. Relative free energies (ΔG, kcal/mol) for reactant complexes **CM1**, **CM2**, and **CM3** (bond distances in Å).

DOI: 10.1021/acs.joc.5b00180
J. Org. Chem. 2015, 80, 3547−3555

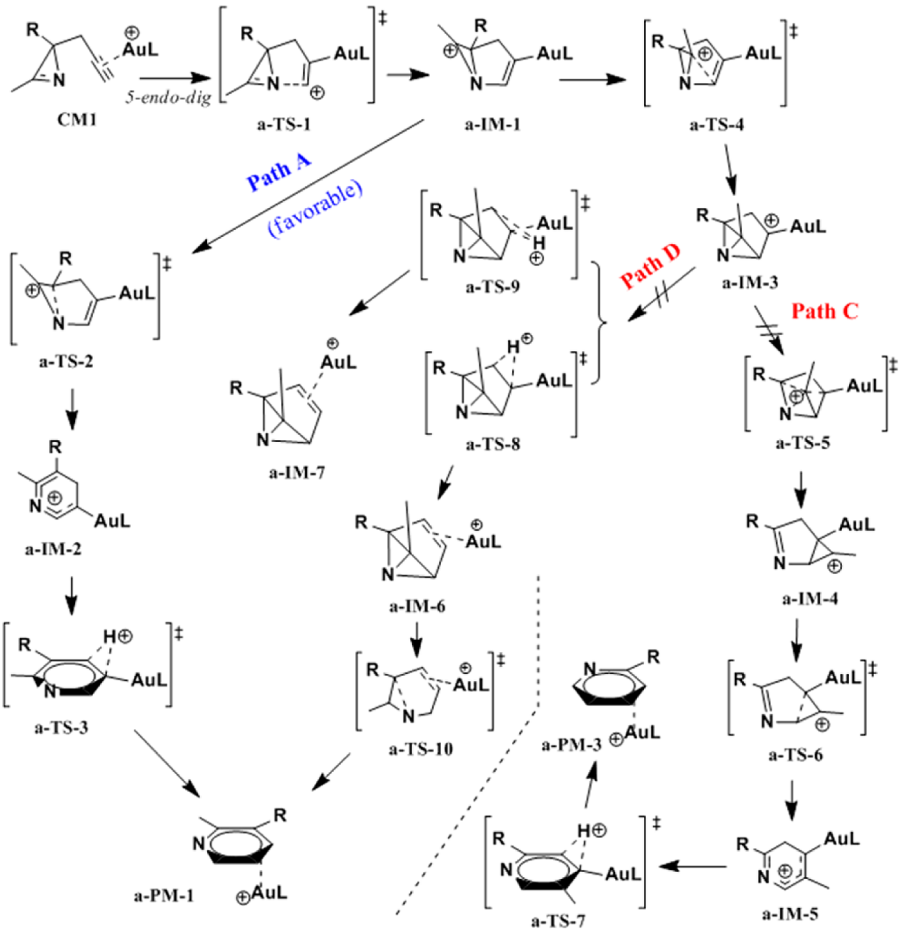

Figure 2. Detailed reaction processes for three possible pathways (paths A, C, and D) promoted by one gold(I) catalyst.

aromatization through 1,2-proton transfer was very easy with only a small free energy barrier ($\Delta G^{\ddagger}$ = 1.19 kcal/mol). Finally, it is dramatically exergonic in the formation of product complex **a-PM-1**.

Additionally, to verify the suggested "concerted" mechanism (path B), as shown in the Introduction, we also started from **a-IM-1** to test this possibility. However, regardless of the initial transition state structures we suggested, both the imaginary vibration of transition states and IRC tracking reveal that only one mode (ring expansion or proton-transfer, see Figure 4) can be detected. Thus, the suggested "concerted" mechanism, including simultaneous ring expansion and proton-transfer, starting from **a-IM-1** is unlikely.

3.1.4. Processes after C1−C5 Bond Formation (Paths C and D). Alternatively, the other possible process is electrophilic attack of the carbocation at the double bond to construct a C1−C5 bond, leading to gold carbenoid intermediate **a-IM-3** (Figure 5). The corresponding transition state **a-TS-4** was located at 2.133 Å of C1−C5 bond distance and 96.42° of C1−N−C5 bond angle, indicating that the two planes (five-membered and three-membered rings) are almost perpendicular. The imaginary vibrational frequency (263.05i cm^{-1}) is mainly associated with the C1−C5 bond stretch mode. In **a-IM-3**, two three-membered rings share one edge (N−C5 bond), and bond distances of C1−C5 and N−C5 are 1.552 and 1.408 Å, respectively. Note that the formation of the stable gold carbenoid **a-IM-3** would beneift from the strong back-donation of gold. $\Delta G^{\ddagger}$ of **a-TS-4** is only 4.98 kcal/mol higher than that of **a-TS-2**, indicating that it might be somewhat competitive to undergo C4−N ring expansion and C1−C5 bond formation from **a-IM-1**. Next, we explored two possible pathways (paths C and D) from intermediate **a-IM-3** to provide more information about the title reaction.

According to the process of cyclopropene-containing 1,5-enyne, a 1,3-carbocationic migration pathway would exist in the reaction and control product selectivity. Figure 5 also shows the corresponding structures and relative free energies. Starting from **a-IM-3**, the carbocation (C5) migrates to connect with the C1 and C2 atoms via double cleavage of the N−C4 and C4−C5 bonds. It would need ∼24.11 kcal/mol to overcome the corresponding transition state **a-TS-5**. After that, compared with **a-IM-1**, **a-IM-4** has a skeleton similar to one carbocation. Likewise, ring expansion followed by proton-transfer would also occur in this pathway. It was found that both steps are rapid ($\Delta G^{\ddagger}$ < 10 kcal/mol). Accordingly, the high free energy barrier (24.11 kcal/mol) of **a-TS-5** could block the path C reaction. Additionally, we could not locate the nonclassic carbocation as found in the case of cyclopropene-containing 1,5-enyne (Figure 6). The reason for the transformation could be attributed to the strong interaction between the electron-deficient carbocation and the electron-rich nitrogen atom.

Also starting from **a-IM-3**, except for the carbocation migration (path C) and the reverse process (path A) mentioned above, 1,2-proton transfer (from C3 to C2) followed by ring expansion (path D) is also tested in this work. As shown in Figure 7, proton-transfer on two different faces has close free energy barriers (∼20 kcal/mol). We think the closed barriers would be

DOI: 10.1021/acs.joc.5b00180
J. Org. Chem. 2015, 80, 3547−3555

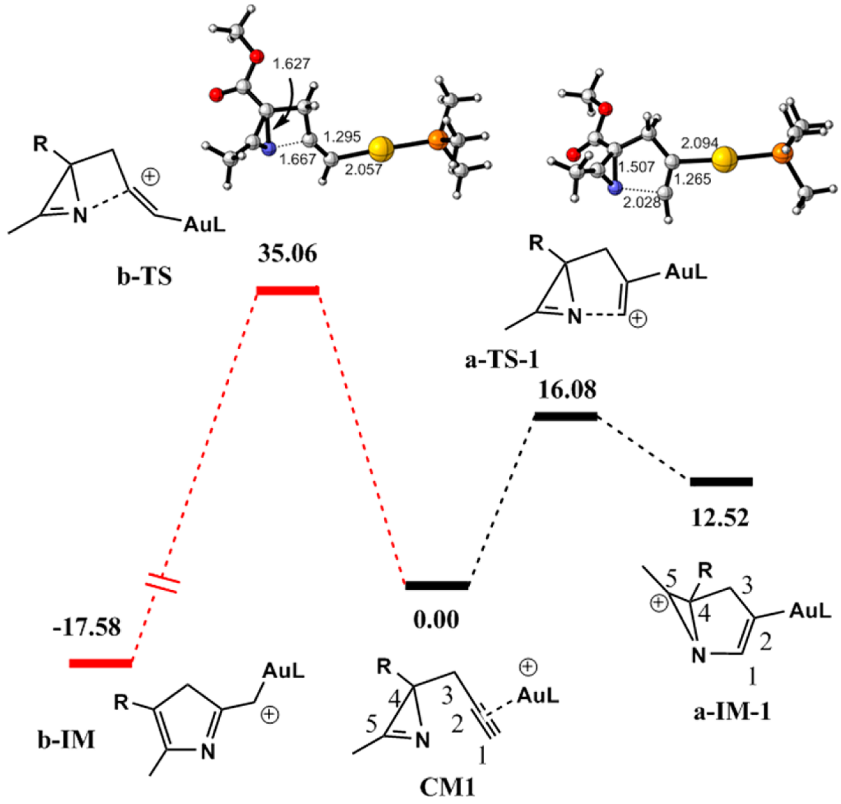

Figure 3. Relative free energy (kcal/mol) profiles in 4-*exo*-dig and 5-*endo*-dig cyclization processes (bond distances in Å).

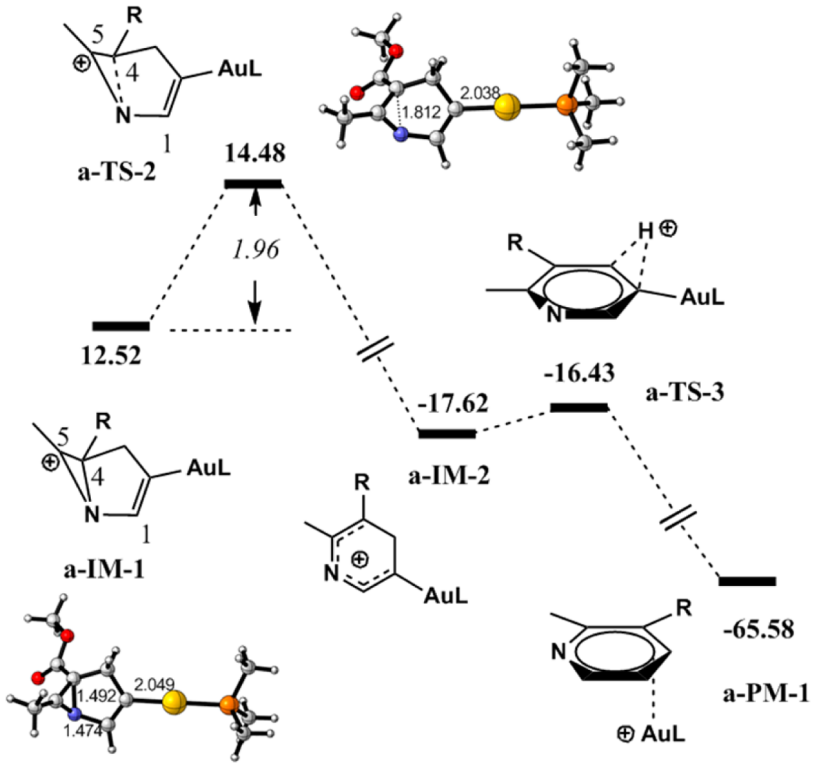

Figure 4. Relative free energy (kcal/mol) profile in path A (bond distances in Å).

rational due to little spatial hindrance using a simplified catalyst and a small substituent at the C5 position. Next, we selected one more stable intermediate (**a-IM-6**) to explore ring expansion. The $\Delta G^{\ddagger}$ of transition state **a-TS-10** is too high (28.54 kcal/mol) to undergo this ring-expansion process. In addition, starting from **a-IM-3**, the "concerted" mechanism, including simultaneous proton-transfer and ring expansion (path B), was also analyzed. Results indicate that this concerted mechanism could also not be

DOI: 10.1021/acs.joc.5b00180
J. Org. Chem. 2015, 80, 3547−3555

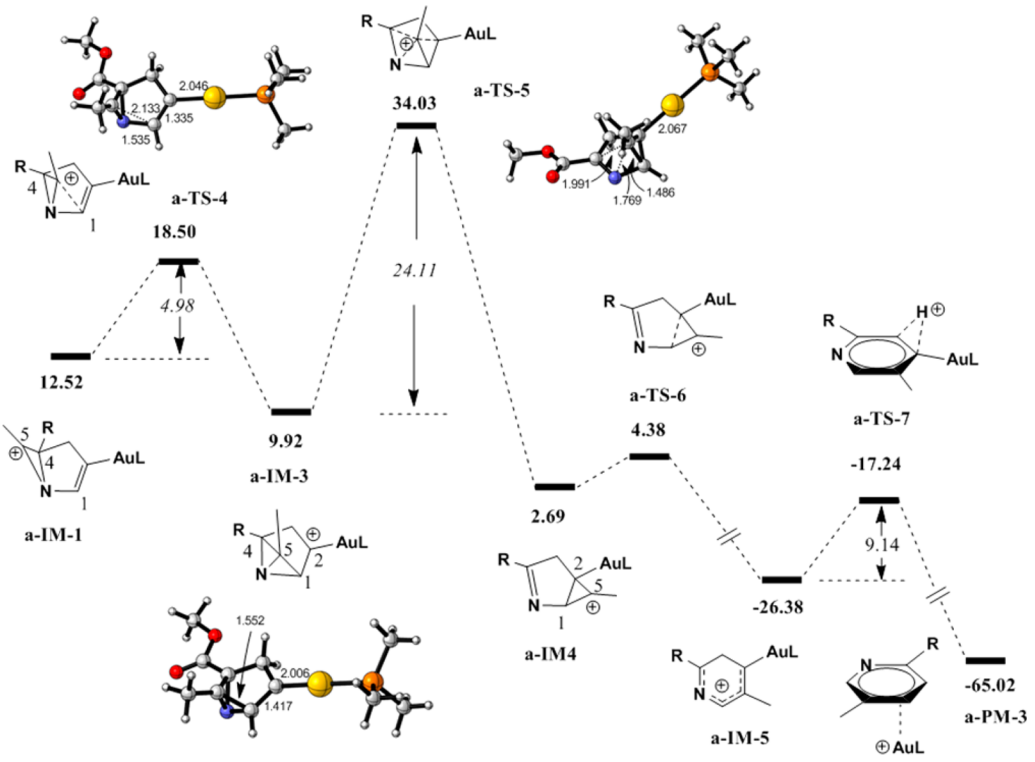

Figure 5. Relative free energy (kcal/mol) profile in path C (bond distances in Å).

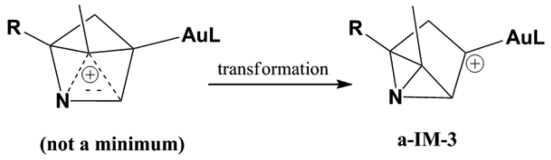

Figure 6. Schematic diagram of for the transformation of a nonclassic carbocation.

found on the potential energy surface. Overall, the high free energy barriers reveal that it would be unlikely for the reaction to proceed via path D.

*3.1.5. Possible Reaction Process from Reaction Complex **CM3** (Path E).* As mentioned above, **CM3** is more stable than **CM1**. Therefore, we attempted to obtain some possible processes starting from **CM3**. Figure 8 shows some possible geometries in our test. Unfortunately, ring-opening gold(I)-nitrene intermediate **A** was not found to be a minimum, which differs from the cases catalyzed by Rh(I) and Fe(II) compounds.[5] Furthermore, although intermediate **C** is unsuccessful in locating the cyclic transition state via nucleophilic addition of nitrogen to alkyne, its relative energy (35.57 kcal/mol at the PBE0/BS-I level) is rather high in the absence of alkyne activation (see the Supporting Information). Another possible geometry (**B**) is also unstable on the potential energy surface and can relax to **C**. That is to say, provided that the gold(I) catalyst interacts with nitrogen of 2*H*-azirine, it would be impossible to catalyze the rearrangement process, which is in agreement with the experiment data in

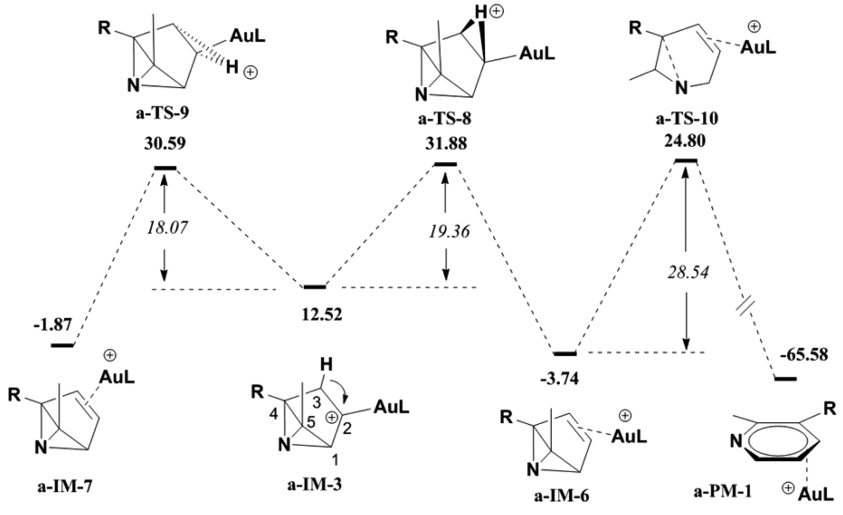

Figure 7. Relative free energy (kcal/mol) profile in path D.

DOI: 10.1021/acs.joc.5b00180
J. Org. Chem. 2015, 80, 3547−3555

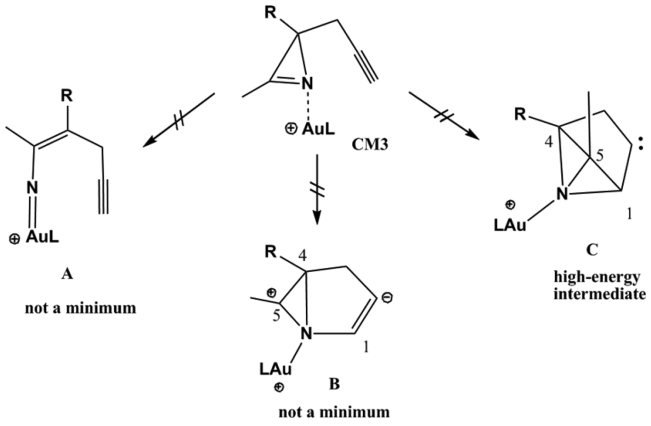

Figure 8. Possible structures in the process starting from **CM3**.

which no reaction occurred without the alkynyl chain in a substrate.[6]

Overall, after the formation of intermediate **a-IM-1** via 5-*endo*-dig cyclization, our computational results support sequential pathway (path A), where ring expansion takes place before proton-transfer, and suggested concerted-type pathway B cannot be optimized in the reaction even though proton transfer is very fast. Starting from intermediate **a-IM-3**, it would be difficult for two other possible pathways (paths C and D) to occur due to much higher energy barriers. In this sense, if intermediate **a-IM-3** was formed in the reaction, it would still reverse and enter the favored path A. Therefore, no matter how high $\Delta G^{\ddagger}$ of transition state **a-TS-4** gets, the title reaction only goes through **a-TS-2** for ring expansion. Additionally, if the dead-end reactant complex **CM3** is formed, it must transform to **CM1** to catalyze the title reaction.

3.2. Influence of the Substituent Group at the Propargylic Position. To provide more information on the title reaction, we tested the substituent groups (methyl, ethyl, or isopropyl) at the propargylic position (C3) to understand their influence on reactivity. Figure 9 shows two types of conformers (*syn* and *anti*). Note that, due to the spatial repulsion between the catalyst and the R group, structures of **anti-CM1** cannot be optimized and transformed to **anti-CM2** when R is an ethyl or isopropyl group. In this sense, the corresponding energies

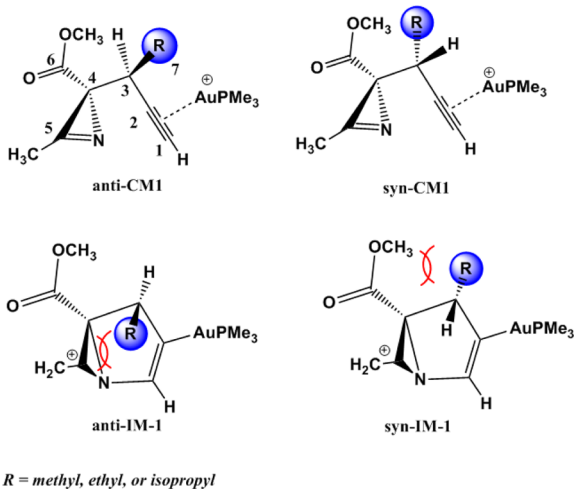

Figure 9. Schematic structures of **syn-CM1**, **anti-CM1**, **syn-IM-1**, and **anti-IM-1**.

relative to **syn-CM3** (or **anti-CM3**) in favored path A are shown in the Supporting Information (Table S6). It is found that the relative Gibbs free energies of **syn-TS1**, **syn-IM-1**, and **syn-TS2** are slightly higher (~1.5−3 kcal/mol) than those of **anti-TS1**, **anti-IM-1**, and **anti-TS2**, which can be explained by steric hindrance between the R group and $-CO_2CH_3$, because the dihedral angle of C6−C4−C3−C7 is close to 0 in the carbocation intermediate **syn-IM-1**. On the other hand, the repulsion between the R and carbocation groups in **anti-IM-1** also has little effect on the relative energies. In addition, our results indicate that the real, large ligand *t*BuXPhos would favorably occupy the *syn* face to efficiently promote the reaction (see Figure 10 and details in the next section). In this way, it would render large repulsion between the real ligand and the R group if the substrate possesses a substituent group at the propargylic *syn* position. Therefore, we assume that the selectivity of product (*anti* > *syn*) would originate from both the ligand effect and the stability of the carbocation.

3.3. Favored Process in the Real System. To evaluate the spatial effect of ligands, we investigated the real system (R_1 = CH_3, R_2 = H, MG = H) as shown in Scheme 3. According to the mechanistic scenario as described above, we only considered favored pathway A for the real system. Note that the fast proton-transfer step is also neglected in the computations. Figure 10 shows the corresponding optimized structures. One can see that the key structural parameters are very similar to those in the simplified models. That is to say, without consideration of the spatial effect, it is rational to assume that the simplified ligand (PMe_3) mimics the real ligand. However, the rate-determining step changes from 5-*endo*-dig in the model system to C−N bond cleavage of ring expansion in the real system.

Furthermore, two phenyl-substituted real systems are also considered to evaluate the electronic effects. The corresponding optimized structures are shown in the Supporting Information. For case 1 (R_1= phenyl, R_2 = H, MG = H), the phenyl group is placed at the C5 position in the azirine motif, whereas for case 2 (R_1 = CH_3, R_2 = phenyl, MG = H), the phenyl group is placed at the alkyne terminal (C1 position). As shown in Table 1, compared with the nonsubstituted reaction, both $\Delta G^{\ddagger}$ of the first step (5-*endo*-dig cyclization) increase by 2−3 kcal/mol in the substituted reactions, which can be attributed to electron delocalization reducing the nucleophilic/electrophilic activity. For case 1, the phenyl group at the C5 atom can stabilize the carbocation in intermediate **r-IM-1**, leading to the decrease in the corresponding energy. Therefore, the rate-determining step becomes 5-*endo*-dig cyclization in case 1. For case 2, the repulsion between phenyl (at the C1 position of alkyne) and tertiary butyl of the ligand would push the free energy barrier slightly higher. From **r-CM1** to **r-IM-1** in case 2, the phenyl group rotates ~60°, making phenyl and tertiary butyl approach each other. Therefore, for the transition state of ring-expansion in case 2, the distance between the phenyl and tertiary butyl groups would be slightly suppressed along with ring-expansion, resulting in more repulsion. Accordingly, $\Delta G^{\ddagger}$ of ring expansion in case 2 is 6.94 kcal/mol from the intermediate, and the overall $\Delta G^{\ddagger}$ reaches 21.79 kcal/mol, which is higher than the other two real reaction systems described above.

Unfortunately, our computational $\Delta G^{\ddagger}$ does not match the experimental observations.[8] In the experiment, the authors found that the rate of the C1-substituted reaction (case 2, 90% yield after 1.5 h) is faster than that of both the C5-substituted (case 1, 79% yield after 48 h) and nonsubstituted reactions (74% yield after 24 h). However, our computational results show that the

DOI: 10.1021/acs.joc.5b00180
J. Org. Chem. 2015, 80, 3547−3555

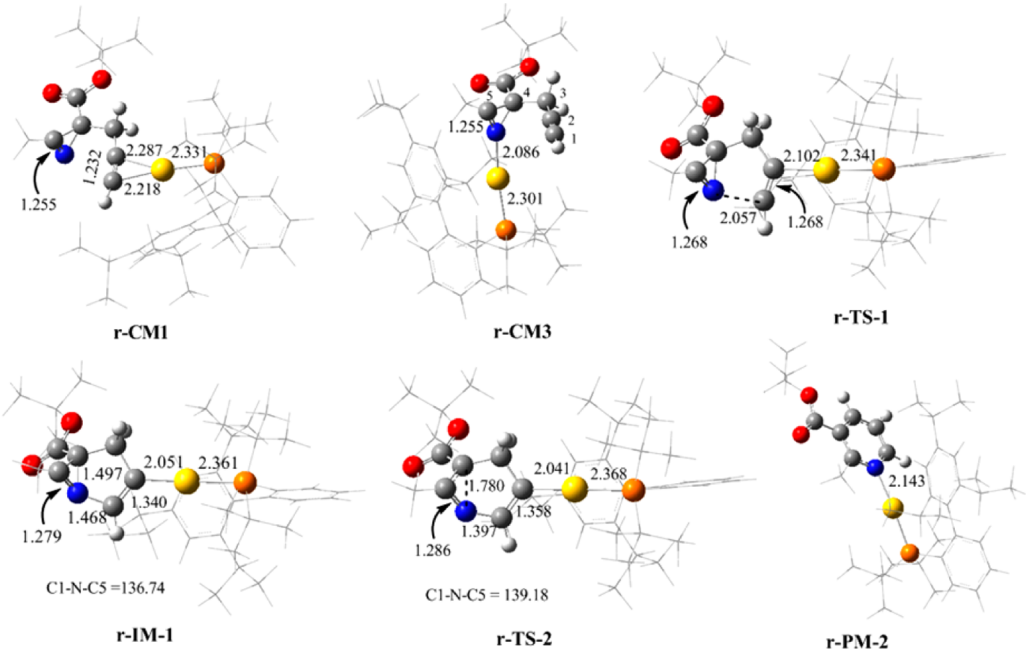

Figure 10. Optimized structures in the rearrangement process of the real system (bond distances in Å).

Table 1. Relative Energies and Free Energies (kcal/mol) for Three Real Reactions

	$R_1 = CH_3$, $R_2 = H$		$R_1 = C_6H_5$, $R_2 = H$		$R_1 = CH_3$, $R_2 = C_6H_5$	
	ΔE	ΔG	ΔE	ΔG	ΔE	ΔG
r-CM3	−5.87	−5.97	−6.29	−5.29	−5.90	−5.96
r-CM1	0.00	0.00	0.00	0.00	0.00	0.00
r-TS-1	13.49	13.76	12.18	15.06	13.54	16.67
r-IM-1	9.72	12.19	5.48	8.20	11.83	14.85
r-TS-2	12.46	15.70	9.39	12.55	17.41	21.79
r-PM-2	−86.08	−82.57	−82.12	−77.48	−78.10	−73.22

reaction of case 2 has higher relative free energy from **r-CM3** (27.75 kcal/mol). We therefore turn our attention to the binding energy of product complexes. We found that the binding energy of the product complex would have an important effect on the reaction rate. As shown in the Supporting Information (Table S4), CH_3 and phenyl at the C5 and C1 positions, respectively, in case 2 result in more repulsion between product and ligand in the product complex (**r-PM-2**). Compared to case 1, the binding energy of **r-PM-2** in case 2 decreases by ∼5.5 kcal/mol. Accordingly, it is easy to exchange product for reactant in the reaction of case 2, whereas for the other two reactions need more time for product exchange due to their binding energies of product complexes being higher than those of the reactant complexes.

4. CONCLUSION

We have investigated the whole mechanism for gold(I)-catalyzed rearrangement of 2-propargyl 2*H*-azirines to pyridines using the DFT method. Five possible pathways have been explored for the reaction. Our results indicate that the arrangement reaction could be efficiently promoted by the gold(I) catalyst through the favored sequential pathway (path A). After 1,5-*endo*-dig cyclization by nucleophilic attack, direct ring expansion (C−N bond cleavage) followed by 1,2-proton transfer could furnish pyridine in the reaction. Because of the *anti* or *syn* conformer of the migration group (MG), the selectivity of product could be explained by the hindrance of ligand (*t*-BuXPhos) and stability of the carbocation. Moreover, the suggested concerted reaction mechanism (path B), including simultaneous ring-expansion and proton transfer, could not be optimized. We found that the binding energy between the product and gold(I) catalyst could account for the observed reaction rate.

■ ASSOCIATED CONTENT

Supporting Information

Selected NBO results, all relevant structures, relative energies, and Cartesian coordinates. This material is available free of charge via the Internet at http://pubs.acs.org.

■ AUTHOR INFORMATION

Corresponding Authors

*E-mail: xzhao@mail.xjtu.edu.cn. Tel: 86 29 8266 5671. Fax: 86 29 8266 8559.
*E-mail: specwy@mail.xjtu.edu.cn.

Notes

The authors declare no competing financial interest.

■ ACKNOWLEDGMENTS

This work was supported by the National Natural Science Foundation of China (No. 21171138), the National Key Basic Research Program of China (No. 2012CB720904), and the Fundamental Research Funds for the Central University.

DOI: 10.1021/acs.joc.5b00180
J. Org. Chem. 2015, 80, 3547−3555

REFERENCES

(1) Huang, C. Y.; Doyle, A. G. *Chem. Rev.* **2014**, *114*, 8153−8198 and citations therein.

(2) (a) Khlebnikov, A. F.; Novikov, M. S. *Tetrahedron* **2013**, *69*, 3363−3401. (b) Khlebnikov, A. F.; Novikov, M. S.; Pakalnis, V. V.; Iakovenko, R. O.; Yufit, D. S. *Beilstein J. Org. Chem.* **2014**, *10*, 784−793. (c) Rostovskii, N. V.; Novikov, M. S.; Korneev, S. M.; Iakovenko, R. O.; Yufit, D. S. *Org. Biomol. Chem.* **2013**, *11*, 5535−5545. (d) Sharma, P.; Kumar, A.; Sahu, V. *J. Phys. Chem. A* **2010**, *114*, 1032−1038. (e) Candito, D. A.; Lautens, M. *Org. Lett.* **2010**, *12*, 3312−3315. (f) Li, X.; Du, Y.; Liang, Z.; Li, X.; Pan, Y.; Zhao, K. *Org. Lett.* **2009**, *11*, 2643−2646.

(3) (a) Neber, P. W.; Hartung, K.; Ruopp, W. *Chem. Ber.* **1925**, *58*, 1234. (b) Nunes, C. M.; Reva, I.; Pinho e Melo, T. M. V. D.; Fausto, R.; Šolomek, T.; Bally, T. *J. Am. Chem. Soc.* **2011**, *133*, 18911−18923. (c) Cardoso, A. L.; Gimeno, L.; Lemos, A.; Palacios, F.; Pinho e Melo, T. M. V. D. *J. Org. Chem.* **2013**, *78*, 6983−6991. (d) Nunes, C. M.; Reva, I.; Fausto, R. *J. Org. Chem.* **2013**, *78*, 10657−10665. (e) Davis, F. A.; Deng, J. *Org. Lett.* **2007**, *9*, 1707−1710.

(4) (a) Inui, H.; Murata, S. *J. Am. Chem. Soc.* **2005**, *127*, 2628−2636. (b) Zhang, X.; Sarkar, S. K.; Weragoda, G. K.; Rajam, S.; Ault, B. S.; Gudmundsdottir, A. D. *J. Org. Chem.* **2014**, *79*, 653−663. (c) Jiang, Y.; Park, C. M.; Loh, T. P. *Org. Lett.* **2014**, *16*, 3432−3435. (d) Okamoto, K.; Mashida, A.; Watanabe, M.; Ohe, K. *Chem. Commun.* **2012**, *48*, 3554−3556.

(5) (a) Jana, S.; Clements, M. D.; Sharp, B. K.; Zheng, N. *Org. Lett.* **2010**, *12*, 3736−3739. (b) Wu, C.; Li, J.; Yan, B. *Dalton Trans.* **2014**, *43*, 5364−5374 and citations therein. (c) Chiba, S.; Hattori, G.; Narasaka, K. *Chem. Lett.* **2007**, *36*, 52. (d) Li, T.; Xin, X.; Wang, C.; Wang, D.; Wu, F.; Li, X.; Wan, B. *Org. Lett.* **2014**, *16*, 4806−4809.

(6) For selected recent reviews on gold catalysis, see: (a) Qian, D.; Zhang, J. *Chem. Soc. Rev.* **2015**, *44*, 677−698. (b) Xie, J.; Pan, C.; Abdukader, A.; Zhu, C. *Chem. Soc. Rev.* **2014**, *43*, 5245−5256. (c) Hashmi, A.; Stephen, K. *Acc. Chem. Res.* **2014**, *47*, 864−876. (d) Zhang, L. *Acc. Chem. Res.* **2014**, *47*, 877−888. (e) Wang, Y. M.; Lachner, A. D.; Toste, F. D. *Acc. Chem. Res.* **2014**, *47*, 889−901. (f) Obradors, C.; Echaavarren, A. M. *Acc. Chem. Res.* **2014**, *47*, 902−912. (g) Zhang, D. H.; Tang, X. Y.; Shi, M. *Acc. Chem. Res.* **2014**, *47*, 913−924. (h) Fuerstner, A. *Acc. Chem. Res.* **2014**, *47*, 925−938. (i) Alcaide, B.; Almendros, P. *Acc. Chem. Res.* **2014**, *47*, 939−952. (j) Fensterbank, L.; Malacria, M. *Acc. Chem. Res.* **2014**, *47*, 953−965. (k) Yeom, H. K.; Shin, S. *Acc. Chem. Res.* **2014**, *47*, 966−977.

(7) Selected examples: (a) Shi, F. Q.; Li, X.; Xia, Y. Z.; Zhang, L. M.; Yu, Z. X. *J. Am. Chem. Soc.* **2007**, *129*, 15503−15512. (b) Gourlaouen, C.; Marion, N.; Nolan, S. P. *Org. Lett.* **2009**, *11*, 81−84. (c) Dudnik, A.; Xia, Y. Z.; Li, Y. H. *J. Am. Chem. Soc.* **2010**, *132*, 7645−7655. (d) Garayalde, D.; Gomez-Bengoa, E.; Huang, X. *J. Am. Chem. Soc.* **2010**, *132*, 4720−4730. (e) Xia, Y. Z.; Dudnik, A.; Li, Y. H. *Org. Lett.* **2010**, *12*, 5538−5541. (f) Dong, Z.; Liu, C. H.; Wang, Y.; Lin, M.; Yu, Z. X. *Angew. Chem., Int. Ed.* **2013**, *52*, 14157−14161. (g) Zhou, T.; Xia, Y. Z. *Organometallics* **2014**, *33*, 4230−4239.

(8) Prechter, A.; Henrion, G.; dit Bel, P. F.; Gagosz, F. *Angew. Chem., Int. Ed.* **2014**, *53*, 4959−4963.

(9) (a) Li, C.; Zeng, Y.; Zhang, H.; Feng, J.; Zhang, Y.; Wang, J. *Angew. Chem., Int. Ed.* **2010**, *49*, 6413−6417. (b) Zhou, Q.; Li, Y. *J. Am. Chem. Soc.* **2014**, *136*, 1505−1513.

(10) Adamo, C.; Barone, V. *J. Chem. Phys.* **1999**, *110*, 6158−6169.

(11) Kang, R. H.; Chen, H.; Shaik, S.; Yao, J. N. *J. Chem. Theory Comput.* **2011**, *7*, 4002−4011. (b) It is found that, although the dispersion energies calculated by the DFT-D3 code are ∼22 kcal/mol in all relevant optimized geometries in the model system, the relative dispersion energies are too low and have little effect on our results (see Table S5 in the Supporting Information). (c) Grimme, S.; Antony, J.; Ehrlich, S.; Krieg, H. *J. Chem. Phys.* **2010**, *132*, 154104. (d) Grimme, S.; Ehrlich, S.; Goerigk, L. *J. Comput. Chem.* **2011**, *32*, 1456−1465.

(12) Def2-TZVP and Def2-SVP basis sets are taken from EMSL (https://bse.pnl.gov/bse/portal) and shown in the Supporting Information. (a) Weigend, F.; Ahlrichs, R. *Phys. Chem. Chem. Phys.* **2005**, *7*, 3297−3305. (b) Andrae, D.; Haeussermann, U.; Dolg, M.; Stoll, H.; Preuss, H. *Theor. Chim. Acta* **1990**, *77*, 123−141.

(13) Fukui, K. *Acc. Chem. Res.* **1981**, *14*, 363−368.

(14) (a) Cances, E.; Mennucci, B. *J. Math. Chem.* **1998**, *23*, 309−326. (b) Mennucci, B.; Cances, E.; Tomasi, J. *J. Phys. Chem. B* **1997**, *101*, 10506−10517. (c) Cances, E.; Mennucci, B.; Tomasi, J. *J. Chem. Phys.* **1997**, *107*, 3032−3041.

(15) (a) Grimme, S. *J. Chem. Phys.* **2006**, *124*, 34108. (b) Ciancaleoni, G.; Rampino, S.; Zuccaccia, D.; Tarantelli, F.; Belanzoni, P.; Belpassi, L. *J. Chem. Theory Comput.* **2014**, *10*, 1021−1034.

(16) Reed, A. E.; Curtiss, L. A.; Weinhold, F. *Chem. Rev.* **1988**, *88*, 899−926.

(17) Frisch, M. J.; Trucks, G. W.; Schlegel, H. B.; Scuseria, G. E.; Robb, M. A.; Cheeseman, J. R.; Scalmani, G.; Barone, V.; Mennucci, B.; Petersson, G. A.; Nakatsuji, H.; Caricato, M.; Li, X.; Hratchian, H. P.; Izmaylov, A. F.; Bloino, J.; Zheng, G.; Sonnenberg, J. L.; Hada, M.; Ehara, M.; Toyota, K.; Fukuda, R.; Hasegawa, J.; Ishida, M.; Nakajima, T.; Honda, Y.; Kitao, O.; Nakai, H.; Vreven, T.; Montgomery, J. A., Jr.; Peralta, J. E.; Ogliaro, F.; Bearpark, M.; Heyd, J. J.; Brothers, E.; Kudin, K. N.; Staroverov, V. N.; Kobayashi, R.; Normand, J.; Raghavachari, K.; Rendell, A.; Burant, J. C.; Iyengar, S. S.; Tomasi, J.; Cossi, M.; Rega, N.; Millam, M. J.; Klene, M.; Knox, J. E.; Cross, J. B.; Bakken, V.; Adamo, C.; Jaramillo, J.; Gomperts, R.; Stratmann, R. E.; Yazyev, O.; Austin, A. J.; Cammi, R.; Pomelli, C.; Ochterski, J. W.; Martin, R. L.; Morokuma, K.; Zakrzewski, V. G.; Voth, G. A.; Salvador, P.; Dannenberg, J. J.; Dapprich, S.; Daniels, A. D.; Farkas, Ö.; Foresman, J. B.; Ortiz, J. V.; Cioslowski, J.; Fox, D. J. *Gaussian 09*, revision C.02; Gaussian, Inc.: Wallingford, CT, 2009.

(18) *CYLview*, 1.0b; Legault, C. Y. Université de Sherbrooke: Quebec, Canada, 2009 (http://www.cylview.org).

DOI: 10.1021/acs.joc.5b00180
J. Org. Chem. 2015, 80, 3547−3555